



IEEE DG Anti-islanding

Driven by Energy...

A Power Line Signaling Based Technique for Anti-Islanding Protection of Distributed Generators—Part I: Scheme and Analysis

Wilsun Xu, *Fellow, IEEE*, Guibin Zhang, Chun Li, *Member, IEEE*, Wencong Wang, *Student Member, IEEE*, Guangzhu Wang, *Member, IEEE*, and Jacek Kliber, *Student Member, IEEE*

Abstract—Anti-islanding protection of distributed generators (DG) is a significant technical barrier to the emerging DG industry. This paper presents an innovative power line signaling based anti-islanding scheme developed in response to the challenge. The scheme broadcasts a signal from a substation to the DG sites using the distribution feeders as the signal paths. A DG is considered as islanded from the upstream system if the signal cannot be detected at the DG site. The proposed scheme has been evaluated using analytical, simulation and field tests. The results are very promising. This paper presents the main ideas of the scheme and its design considerations. Methods to create and detect the signals are shown and their performances are analyzed.

Index Terms—Distributed generation, distributed generation (DG) interconnection, islanding detection.

I. INTRODUCTION

DISTRIBUTED GENERATION (DG) has recently gained a lot of momentum in the power industry due to market deregulation and environmental concerns. An important requirement to interconnect a DG to power distribution systems is the capability of the generator to detect island conditions. Islanding occurs when a portion of the distribution system becomes electrically isolated from the remainder of the power system, yet continues to be energized by distributed generators. Failure to trip islanded generators can lead to a number of problems to the generators and the connected loads. The current industry practice is to disconnect all distributed generators immediately after the occurrence of islands. Typically, a distributed generator should be disconnected within 100 to 300 ms after loss of main supply [1], [2].

To achieve such a goal, each distributed generator must be equipped with an islanding detection device, which is also called

anti-islanding device. The common devices used for this purpose are the modified versions of the under/over voltage and under/over frequency relays such as the rate of change of frequency relay (ROCOF) and the vector surge relay (VSR) [3]. These relays work on the principle that a power imbalance in the islanded system will lead to frequency drift. However, they cannot function properly or fast enough if the generation and load mismatch is small [4].

In order to overcome the above problem, a few schemes that require a DG to inject small disturbances to the system have been proposed [5], [6]. Some of them have gained acceptance for inverter-based DGs. However, no active schemes have been fully developed for synchronous machine based DGs. Another main challenge facing the active schemes is the interaction among the DGs that introduce similar disturbances to the system. At present, there is no answer to this question.

In addition to the above local information based schemes, techniques that use telecommunication means to trip islanded DGs have been used in industry [7]. In addition to high cost, such a ‘transfer trip’ scheme can be very complicated as well. For example, each openable device between the DG and the supply system needs a transmitter. Some of the devices need to be reconfigured and equipped with the capability of interfacing with the signal transmitter. If telecommunication coverage is weak or non-existent, the cost of a transfer trip scheme alone could kill a DG project.

Over the past several years, anti-islanding protection for DG has emerged as one of the most challenging technical barriers for DG interconnection, especially for synchronous generators connected at medium voltages. Many research projects have been conducted to solve the problem worldwide. Reference [8], [9] provides a good review on this issue.

This paper presents a fundamentally different approach for DG anti-islanding protection. The scheme continuously broadcasts a signal from the utility substation to the downstream DGs. As a result, it transforms the detection of islanded DGs into the check of signal continuity between the substation and the DG sites. This scheme is quite unique as it combines the advantages of the transfer trip and local detection schemes. Power line is used as a communication medium. The scheme is intended for synchronous machine based DGs connected to primary distribution systems. It has been investigated for more than 3 years including extensive field evaluations. The results have been quite promising. The objective of this paper is to present key ideas of the scheme and their analysis. Field test results will be reported in a companion paper.

Manuscript received April 3, 2006; revised June 7, 2006. This work was supported in part by the Alberta Energy Research Institute and four utility companies in Alberta (ATCO, Epcor, Enmax, and FortisAlberta). Paper no. TPWRD-00174-2006.

W. Xu, G. Zhang, W. Wang, and J. Kliber are with the Department of Electrical and Computer Engineering, University of Alberta, Edmonton AB T6G 2V4, Canada (e-mail: wxu@ee.ualberta.ca).

C. Li is with Hydro One, Toronto, ON M5G 1P5, Canada (e-mail: chunli@ieee.org).

G. Wang is with the School of Electrical Engineering, Shandong University, Jinan 250061, China (e-mail: sdwgz@sdu.edu.cn).

Color versions of one or more of the figures in this paper are available online at <http://ieeexplore.ieee.org>.

Digital Object Identifier 10.1109/TPWRD.2007.899618

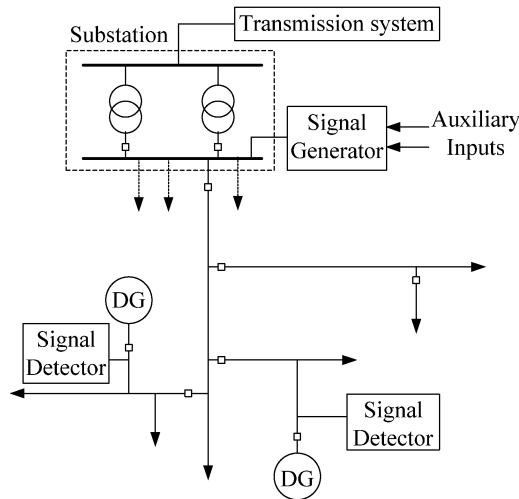


Fig. 1. Illustration for the proposed anti-islanding scheme.

II. DESCRIPTION OF THE PROPOSED SCHEME

The proposed scheme shown in Fig. 1 includes two devices: a signal generator (SG) connected to the substation bus and a signal detector (SD) at the terminal of a given DG. The signal generator broadcasts a signal to all distribution feeders with a preset protocol continuously. If the detector of the DG does not sense the signal (caused by the opening of any devices between the substation and the DG) for certain duration, it is considered as an island condition and the DG can be tripped immediately. If the substation bus loses power, which is another islanding condition, the signal generator also loses power and stops broadcasting. So that downstream DGs will also trip. Furthermore, the signal generator has several auxiliary inputs. Any one of the inputs can stop the broadcast, resulting in tripping all DGs in the system. This feature is particularly useful when transmission system operators need to trip the DGs. It is also useful if a transmission system island is formed.

This scheme works like a transfer trip scheme. However, since power line is used as signal carrier, the opening of any devices can be detected automatically. It works independent of network topology changes (feeder reconfiguration). The scheme is also economical since one SG installed at the substation can satisfy the need of all the downstream DGs. Another important advantage is that the scheme can be tested without actually breaking up the distribution feeders. The main tests could be done by simply stopping the signal generator. The signal detectors should detect null signal in this case.

A. Signal Generator (SG)

Some mature techniques are available to send signals and even information over power lines. Examples include ripple control technique, waveform shift technique and waveform distortion technique [10]–[12]. For islanding detection purpose, the signaling technique should be reliable, low cost and have a fast response. It is also desirable to have minimum interference with power communication schemes that already exist in a distribution system. After extensive evaluation on various schemes, the waveform distortion technique is chosen as the means to broadcast signals.

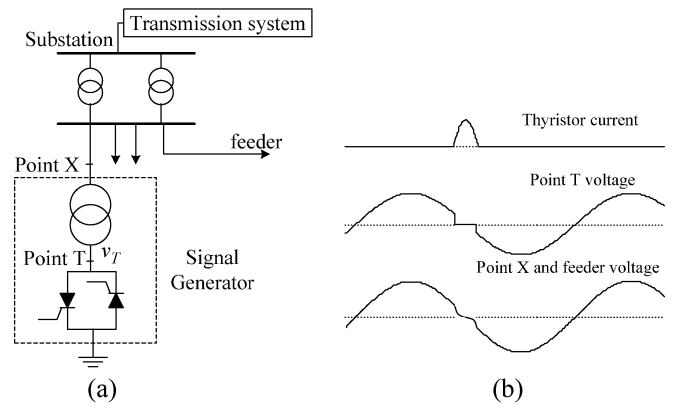


Fig. 2. Signaling method and resulting waveforms.

Principle of the waveform distortion technique is shown in Fig. 2(a) [12]. A step down transformer (also called signal transformer) reduces the secondary side voltage of the substation to a level for thyristor operation. It also limits short circuit current and voltage distortion when the thyristor is turned on. The thyristor turns on several degrees before its voltage crosses zero, creating a momentary short circuit. The thyristor automatically turns off when its current reverses direction. Fig. 2(b) shows the resulting waveforms. It can be seen that there is a small distortion around the zero crossing point of primary feeder voltage. This distortion voltage is the signal. If the thyristor does not fire, there is no waveform distortion and thus no signal.

To facilitate detection, the anti-islanding signal can be assigned certain patterns. For example, it can be broadcast for every 2, 3 or 4 cycles and through a certain channel, say, phase A to Ground (denoted as A-G channel), B-G, or C-G. Phase-to-phase channels (A-B, B-C or C-A) are also available, in which a thyristor is connected and fired between two phases to create signals over the phase-phase voltage. Two anti-parallel thyristors can be used to fire at the voltage rising or falling edges so more signal patterns are available for use.

B. Signal Detector (SD)

The signal detector installed at the DG terminal examines the presence of the anti-islanding signal and determines if an islanding condition has occurred. A significant feature of the proposed scheme is that the signal is extracted by subtracting two consecutive voltage cycles (Fig. 3). The thyristor is fired in a way such that the voltage distortion exists in only one of two consecutive cycles. The difference between these two cycles is the distortion voltage, i.e. the signal. This subtraction method is extremely powerful since it filters out the background distortion in the voltage waveforms. The scheme is therefore essentially immune to background waveform distortions.

After a voltage distortion signal is extracted, additional algorithms are needed to detect if a signal indeed exists. Details of the signal detection algorithms will be explained in Section V.

III. DESIGN PARAMETERS FOR SIGNAL GENERATOR

There are two key design parameters for the signal generator. One is the size of the signal transformer and the other is the

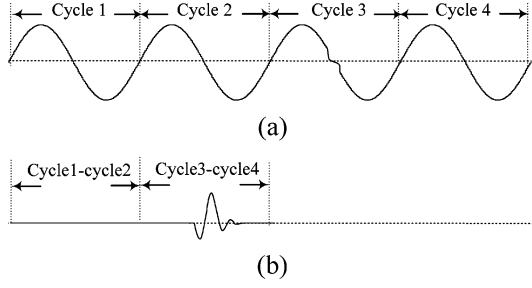


Fig. 3. The subtraction method for signal extraction. (a) Voltage waveform (signal is at the 3rd cycle); (b) voltage distortion signal waveform.

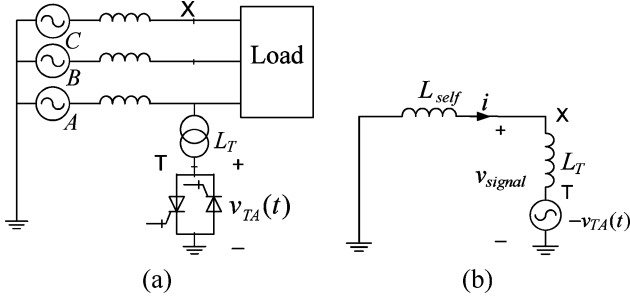


Fig. 4. Analysis of the signaling circuit.

rating of the thyristor. The signal transformer is selected to ensure there is sufficient signal strength. The thyristor is selected to meet voltage and current stress requirements. The case where SG fires between phase A and ground as shown in Fig. 4(a) is used as an example to determine the design parameters. The steady state sinusoidal voltage at the secondary side of the signal transformer when there is no signaling can be expressed as

$$v_{TA}(t) = -\sqrt{2/3}U_N \sin \omega t \quad (1)$$

where U_N is the rated phase-to-phase voltage at the secondary side of signal transformer. According to superposition principle, the signaling process is equivalent to injecting a negative voltage source $-v_{TA}$ between phase A and the ground at point T. The signaling transient can be calculated with a circuit energized by $-v_{TA}$ as shown in Fig. 4(b), where L_{self} is the self-inductance of the supply system at point X, and L_T is the signal transformer inductance. In this circuit, the other two phases are approximated as open circuits, so are the loads connected to the feeders.

If the thyristor is fired ahead of v_{TA} 's zero crossing point by an angle of δ , the thyristor conduction period will be 2δ , and the voltage distortion signal at point X and the thyristor current can be determined as

$$v_{signal}(t) = \sqrt{2/3}U_N \frac{L_{self}}{L_{self} + L_T} \sin \omega t, \quad \omega t \in [-\delta, \delta] \quad (2)$$

$$i(t) = \frac{\sqrt{2/3}U_N}{X_{self} + X_T} [\cos \omega t - \cos \delta] \quad (3)$$

where $X_{self} = \omega L_{self}$ and $X_T = \omega L_T$. The corresponding waveforms are shown in Fig. 5.

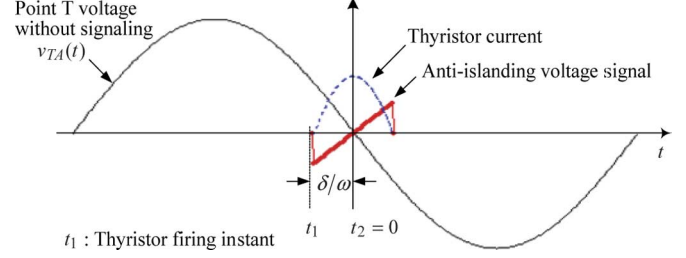


Fig. 5. Waveforms of the anti-islanding signal and thyristor current.

TABLE I
EQUATIONS ABOUT SIGNAL STRENGTH AT POINT X

Signaling channel	Signal strength k (%)
Phase-Ground	$\frac{\sin \delta}{1 + 3x_T S_{PG} / S_T}$
Phase-Phase	$\frac{\sin \delta}{1 + x_T S_{3ph} / S_T}$
S_{3ph} : Supply system three phase fault level at point X; S_{PG} : Supply system phase-to-ground fault level at point X; S_T : Stepdown transformer capacity (three-phase); x_T : Impedance of the stepdown transformer in percentage.	

The peak of $v_{signal}(t)$ represents the strength of the anti-islanding signal, which is

$$V_{signal_peak} = \sqrt{2/3}U_N \frac{L_{self}}{L_{self} + L_T} \sin \delta.$$

Defining the signal strength as the ratio of signal peak to the peak of its carrier voltage, we can obtain

$$k = \frac{V_{signal_peak}}{V_{PG_peak}} = \frac{L_{self} \sin \delta}{L_{self} + L_T} = \frac{X_{self} \sin \delta}{X_{self} + X_T} \times 100\%. \quad (4)$$

If the distribution system in Fig. 4 is grounded through an reactance X_N , the signal strength will be

$$k = \frac{(X_{self} + X_N) \sin \delta}{(X_{self} + X_N) + X_T} \times 100\%. \quad (5)$$

Both (4) and (5) can be converted to the form of Table I by substituting the impedances with the system fault level and the transformer capacity. If the system neutral is grounded through a resistance R_N , the above analytical method still works. However, the signal strength cannot be calculated using (5) unless R_N is much smaller than X_{self} .

Table I summarizes the equations of signal strength P-G and P-P signaling channels. Note that for the P-P signaling, the signal strength is not affected by system grounding condition. These equations can be used to select signaling transformer.

Based on the above analysis, the average and RMS values of the thyristor current can be determined as

$$I_{rms} = \frac{I_{peak}}{\sqrt{N}} \frac{1}{1 - \cos \delta} \times \sqrt{\frac{1}{2\pi} [\delta(2 + \cos 2\delta) - 1.5 \sin 2\delta]} \quad (6)$$

$$I_{average} = \frac{I_{peak}}{N} \frac{\sin \delta - \delta \cos \delta}{\pi(1 - \cos \delta)} \quad (7)$$

TABLE II
 EXAMPLE SG PARAMETERS

k	SD and SG: P-P			SD and SG: P-G		
	S_T (kVA)	I_{peak} (A)	I_{RMS} (A)	S_T (kVA)	I_{peak} (A)	I_{RMS} (A)
3%	102	943	140	116	1246	185
4%	139	1258	187	158	1661	247
5%	177	1572	234	202	2076	308

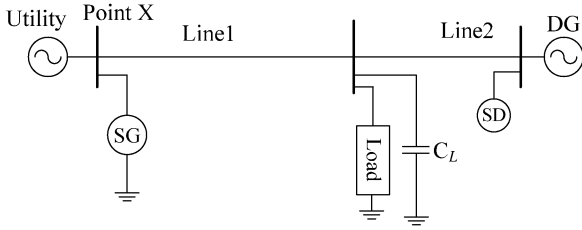


Fig. 6. Single line diagram of the simulation system.

where

$$\begin{aligned}
 I_{peak} &= \frac{\sqrt{2/3}(1 - \cos \delta)}{U_N [1/(3S_{PG}) + x_T/S_T]} \\
 &\quad \text{(Phase-Ground signaling)} \\
 &= \frac{\sqrt{2}(1 - \cos \delta)}{2U_N(1/S_{3ph} + x_T/S_T)} \\
 &\quad \text{(Phase-Phase signaling)}. \tag{8}
 \end{aligned}$$

N stands for the interval between two firing events in the unit of number of cycles. A large N such as 4, 5 or 6 can be used to reduce the heating stress on the thyristor. The side effect is that a larger N may delay the response speed of the signal detector.

As an example, a case where a SG is to be installed at a 12 kV substation bus whose fault level is $S_{PG} = 30.4$ MVA and $S_{3ph} = 79.7$ MVA is considered. If $\delta = 30^\circ$, $x_T = 2\%$, $U_N = 480$ V, $N = 4$ (firing at every 4th cycle), the minimum size of signal transformer and thyristor current are listed in Table II.

IV. SIGNAL CHARACTERISTICS

This section investigates the characteristics of the anti-islanding signal as seen at a DG site. A representative 25 kV distribution system shown in Fig. 6 is used for this purpose. Parameters of the system are listed.

- Utility: 25 kV, impedance 6.25 + j14.4 ohm, Y_g connected.
- Feeders: Line1 is 10 km and Line2 is 1 km; R_1, X_1, R_0, X_0 are 0.2138, 0.3928, 0.3875, 1.8801 ohm/km, respectively, and B_1, B_0 are 4.2315 and 1.6058 Microsiemens/km, respectively.
- DG transformer: 25 k/480 V, Y_g/Δ connection, 6 MVA, impedance 6%.
- DG: 480 V, 5 MVA, impedance 25%; Y_g connected.
- Load: R-L load, 2 MVA; power factor of 0.9.
- Capacitor: 0.8 MVar.
- SG: 3-phase transformer 25/0.48 kV, 150 kVA, impedance 3%; firing angle of 20° ; A-B signaling.

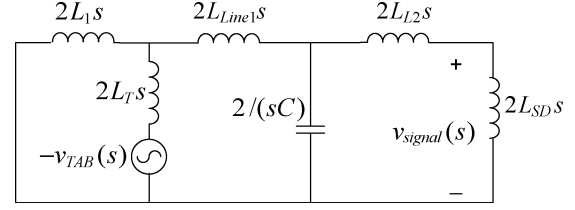


Fig. 7. Equivalent circuit for signal propagation analysis.

- SD: located at the 480 V bus of DG transformer; detection channel is B-G (the P-G channel with the strongest signal).

The equivalent circuit representing the system is shown in Fig. 7. For simplified analysis, both the load and the resistive components are ignored. According to the principle of superposition, the anti-islanding signal at the DG site is the response of the system energized by a virtual voltage source $-v_{TAB}$, where $v_{TAB} = \sqrt{2}U_N \sin \omega t$ is the steady state sinusoidal phase A-B voltage. This source is injected between phase A and B at the secondary side of the SG transformer during thyristor conduction. Symbols $L_1, L_T, L_{Line1}, L_{Line2}, L_{DGxfmr}$ and L_{DG} represent the positive sequence inductances of the utility system, SG transformer, Line1, Line2, DG transformer and DG, respectively. C represents the shunt capacitance. $L_{L2} = L_{Line2} + L_{DGxfmr}$, $L_{SD} = L_{DG}$

The Laplace transformation of anti-islanding signal is determined to be

$$v_{signal}(s) = -v_{TAB}(s) \frac{L_1}{L_1 + L_T} \frac{L_{SD}}{L_{sum}} \frac{1}{1 + (s/\sigma)^2} \tag{9}$$

where

$$\begin{aligned}
 L_{sum} &= L_1/L_T + L_{Line1} + L_{L2} + L_{SD}, \quad \sigma = \sqrt{1/L_{eq}C}, \\
 L_{eq} &= (L_1/L_T + L_{Line1})/(L_{L2} + L_{SD}). \tag{10}
 \end{aligned}$$

According to the above equations, the following conclusions can be drawn.

- The signal at the DG site is initially driven by voltage source $-v_{TAB}(t)$ during the thyristor conduction period. After that, the signal is oscillatory at the system natural frequency of the system σ .
- $-v_{TAB}(s)L_1/(L_1 + L_T)$ represents the signal level at the SG connection point X. The signal strength at DG terminal is reduced according to the ratio of L_{SD}/L_{sum} . It can be seen that a very large DG (meaning a small L_{DG} value) will lead to signal attenuation.

Computer simulations have been carried out to study the anti-islanding signals. Representative signal waveforms are shown in Fig. 8.

To determine which system components have more impact on the characteristics of the signal, key system parameters are varied. The variations of these parameters are shown as percentages of the base case values. Key signal characteristics of interest are the signal peak value, signal attenuation, and its oscillation frequencies.

Fig. 9 shows the signal strength k at the DG site. It can be seen that the impact of line length and load level is not very significant. The utility impedance has a large impact since it is the main factor influencing the voltage distortion level at the SG

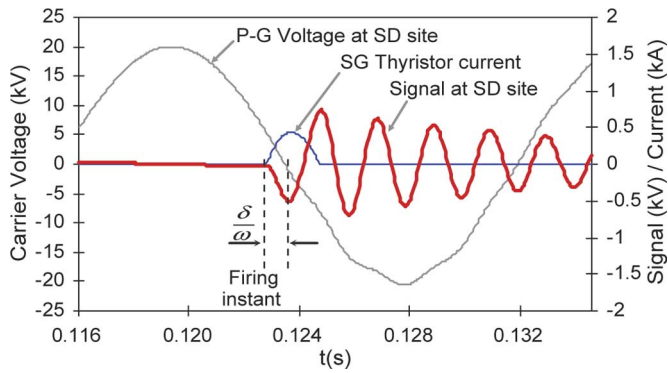


Fig. 8. Representative signal waveforms (all converted to values at 25 kV side).

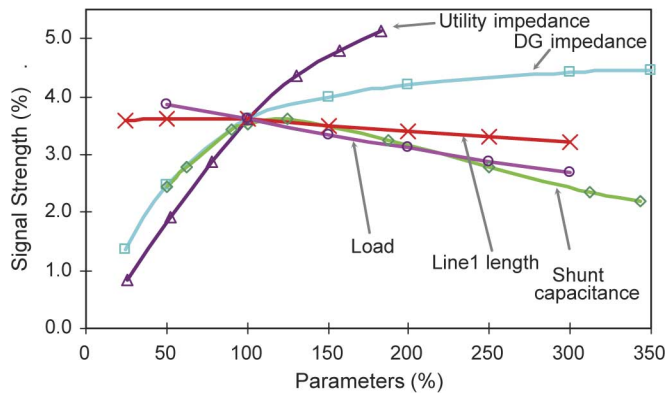


Fig. 9. Signal strengths as affected by system parameters.

site. The impact of the DG impedance can be significant if the impedance becomes quite small. The impact of shunt capacitance is not straightforward. There is a value where the capacitor produces maximum signal level. Detailed analysis of the cause reveals that the phenomenon is related to the natural frequency of the system and the associated resonance situation. It is a coincidence in this case that the peak signal level occurs at 100% capacitor value. The signal RMS value is also determined. It was found that it has similar characteristics to the signal peak value.

Fig. 10 shows the attenuation characteristics of the signal. The attenuation factor is defined as $k_{@DG}/k_{@SG}$. It characterizes the degree of signal reduction when it travels from the substation to the DG site. The attenuation is useful to guide the selection of SG size. The figure shows that the DG impedance (or DG capacity) is the main factor influencing signal attenuation. For the given system, when DGs capacity is lower than 10MVA, the signal attenuation is insignificant. For larger DG installations, a stronger signal generator may be needed. The result also shows that heavy load together with large shunt compensation can also cause notable signal attenuation. The system impedance has a negligible effect on signal attenuation.

The characteristics of signal frequency are shown in Fig. 11. This frequency a critical parameter for the SD algorithm explained later. The frequency is estimated using a duration of three cycles of signal oscillation so it represents the dominant natural frequency of the system. The results show that the size of shunt capacitance affects the frequency most, which is followed by the utility impedance. The Line length and DG impedance

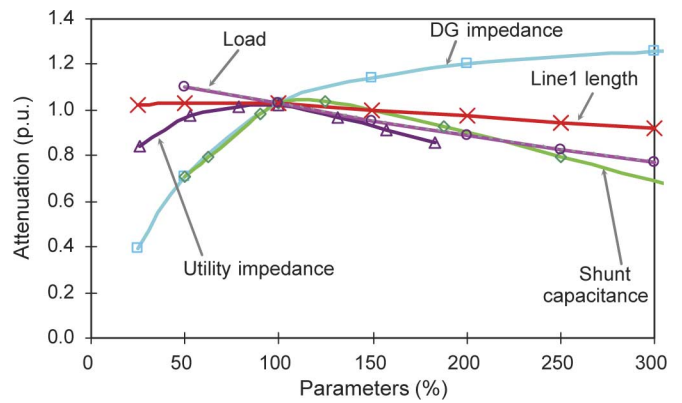


Fig. 10. System attenuation as affected by system parameters.

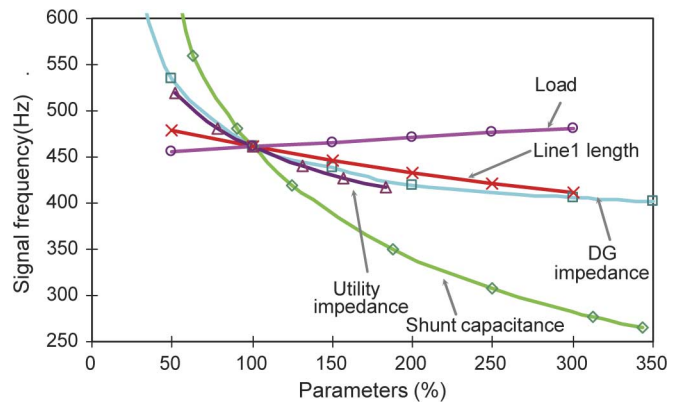


Fig. 11. Signal oscillation frequencies as affected by system parameters.

have mild effects. The load has little effect. The results also reveal that typical signal frequency is within 200 ~ 600 Hz.

The case where SD is installed at the HV voltage side of the DG transformer (at 25 kV) has also been studied. It was found that the signal strength is increased from 3.6% to 4.4%. As a result, connecting SD at the HV side is a very effective way to enhance signal detectability or to reduce the size of signal generator. On the other hand, the SD installation becomes more expensive since primary voltage PTs are needed. The simulation results have been compared with the analytical results in (10). A good agreement between the simulation and analytical results has been found. For example, the calculated oscillation frequency at the base parameters is 461 Hz. It is very close to the simulation results. Due to space limitation, detailed comparison results are not shown. Main conclusion drawn from the comparative studies is that (9) and (10) can be used to estimate the key characteristics of the signal.

V. SIGNAL DETECTION ALGORITHMS

As mentioned in Section II, after the voltage distortion between two consecutive cycles (denoted as v_{signal}) is extracted, an algorithm is needed to detect whether a signal is actually present or not. Based on the characteristics of the signal at the DG site presented in the previous section, three signal detection algorithms are proposed and investigated. The objective is to choose the best algorithm for field implementation.

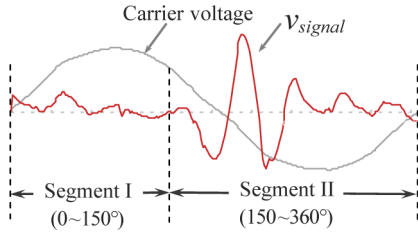


Fig. 12. Detection algorithm based on signal RMS.

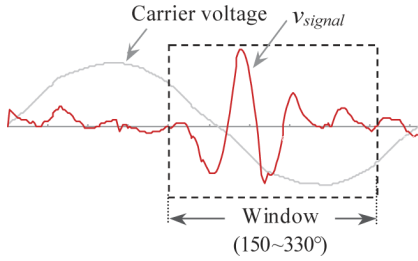


Fig. 13. Detection algorithm based on spectrum.

The first algorithm uses the RMS value of v_{signal} to detect the signal. As shown in Fig. 12, this algorithm divides one fundamental cycle of distortion signal into two segments. Segment I is from 0° to 150° , and segment II from 150° to 360° . With a firing angle of less than 30° , the signal will exist in segment II only. The RMS values of both segments are calculated using

$$RMS = \sqrt{\left(\sum_{i=1}^{N_{seg}} v_{signal_i}^2\right) / N_{seg}} \quad (11)$$

where N_{seg} is the number of all sampled points for one segment. A detection logic can therefore be designed as follows: 1) A normal signal is considered as exist if the RMS value of segment II is higher than preset threshold and that of segment I is lower than another threshold. 2) A signal is considered as nonexistent if the RMS of segment II is lower than a preset threshold. 3) If both RMS values of segments II and I are higher than their corresponding thresholds, the signal is considered abnormal and a warning is triggered. The field test showed that the average signal RMS strength was about 0.85%. A 0.44% threshold is found to give the best detection results for the system tested.

This algorithm is intuitively straightforward. When applied to actual field signals that contain high noise and low signal levels, its performance is not very good. As a result, two alternative algorithms are proposed.

The second algorithm attempts to utilize the oscillatory pattern of the signal for detection. The algorithm works as follows. A portion of the extracted signal is used for DFT analysis. The signal window uses the zero crossing point of the carrier voltage as a reference (Fig. 13). The window has a width of 180° and starts 30° ahead of the voltage zero crossing point. If the signal oscillation frequency were known, one could use the magnitude of the resulting harmonic component whose frequency is closest to the signal oscillation frequency as an index to detect the existence of the signal.

In reality, the signal frequency is not known and is system dependent. The above spectrum based algorithm will make the

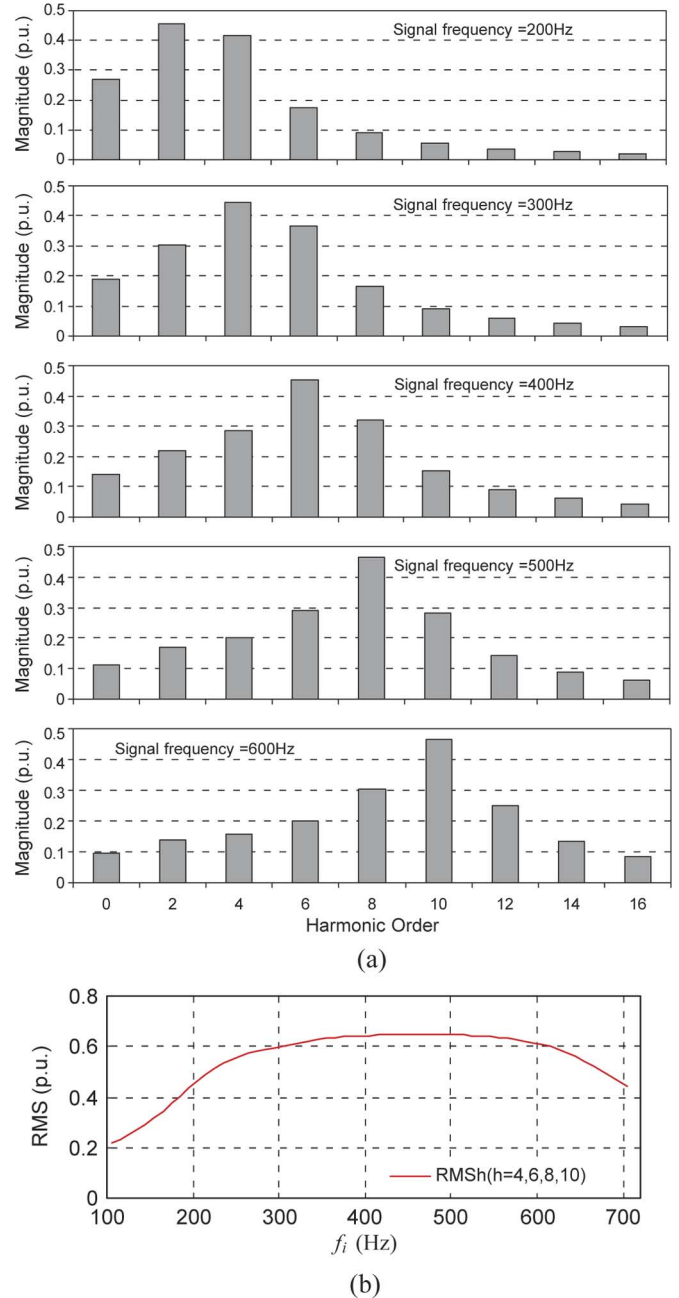


Fig. 14. Detection performance of the spectrum-based algorithm. (a) Harmonic magnitudes as affected by signal frequency. (b) Spectrum RMS_h response to different signal frequencies.

signal detector too system dependent to be practically useful. In addition, the signal frequency may reside between two harmonics. This factor plus the transient nature of the signal waveform make the signal to show up as a group of harmonics in the DFT spectrum (Fig. 14). Therefore, it is important to use a group of harmonic components for signal detection. Based on the field experience, [13] has shown that the natural frequencies of North American distribution systems are between 200 Hz to 600 Hz. As a result, harmonics with order 4, 6, 8, and 10 are selected as a group to form a composite RMS index as follows:

$$RMS_h = \sqrt{M_{h4}^2 + M_{h6}^2 + M_{h8}^2 + M_{h10}^2} \quad (12)$$

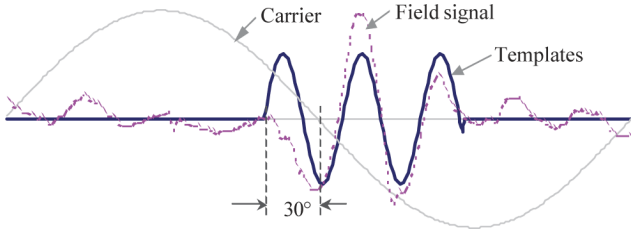


Fig. 15. Waveform of a windowed sinusoidal template.

where M_{hi} is the magnitude of the h_i^{th} harmonic. Note that due to the width of the DFT window used, only even order harmonics exist. A signal is considered as existent if index RMS_h is above a threshold.

The impact of signal frequency on the performance of the proposed algorithm has been investigated. A simulated signal waveform with different oscillation frequencies f_i is input to the spectrum-based algorithm. The resulting spectrums and RMS_h are examined to verify whether RMS_h is an adequate indicator of signal presence. The results are shown in Fig. 14. Fig. 14(a) shows the magnitudes of spectrum components. It can be seen that as f_i varies from 200 to 600 Hz, the highest component appears between the 2nd harmonic to 10th harmonic. Which harmonic exhibits peak value is dependent on the signal frequency. If we taken 4th, 6th, 8th and 10th harmonics into account in the RMS_h form of (9), most signal peaks will be included. Fig. 14(b) shows that RMS_h value. It can be seen that RMS_h varies with respect to the signal oscillation frequency f_i . When f_i is within 200 ~ 600 Hz range, RMS_h has a high response. It suggests that the index is suitable for the intended application. In fact, the RMS_h index filters out low and high frequency noises and could exhibit a better performance than the first algorithm.

The 3rd detection method is to compare the distortion waveform with a signal template $v_{template}$ using the following correlation equation:

$$CR = \left| \sum_i v_{signal_i} v_{template_i} \right| \quad (13)$$

A higher CR index suggests a higher degree of match between the signal and template. A threshold for the CR index is applied to determine if a signal exists. An important consideration for this template-based method is how to select an adequate signal template. A system dependent template will generally improve the reliability of detection. But it makes the signal detector too complicated. After studying various options, a windowed sinusoidal waveform shown in Fig. 15 is selected as the template. The template is aligned to the thyristor firing instant on the voltage waveform. Since the thyristor firing angle is usually fixed (say, 30°), the template position is fixed. Under ideal condition, the frequency of the template sinusoid should be equal to the signal oscillation frequency. This will give almost "perfect" match between the signal and the template. In reality, however, the signal frequency is unknown. To overcome this problem, a set of templates is proposed, each with a different frequency and aligned at the same position. Utilizing the natural frequency data

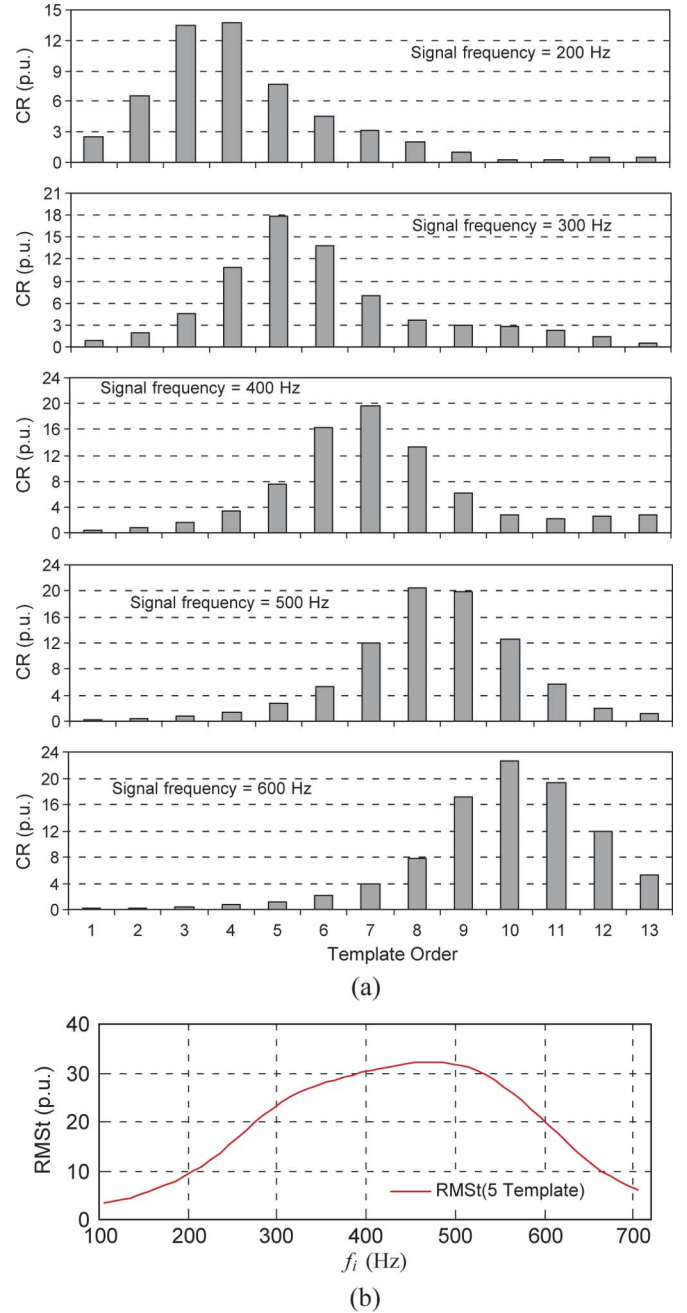


Fig. 16. Detection results of a template-based algorithm. (a) CR indices computed using different templates. (b) Template RMS_t response to different signal frequencies.

of [13], five templates with frequencies equal to 5th, 6th, 7th, 8th and 9th harmonics are selected. The detection index is

$$RMS_t = \sqrt{CR_{t5}^2 + CR_{t6}^2 + \dots + CR_{t9}^2} \quad (14)$$

where CR_{ti} is the calculation result with the i th template.

The impact of signal frequency on the performance of the template-based algorithm has also been investigated as well. The same simulated signal is input to the algorithm. The results are shown in Fig. 16. Fig. 16(a) shows the CR index corresponding to different template orders. As expected, the best

template that yields the highest CR value varies with signal frequency. For the signal frequency range of 200 Hz to 600 Hz, the peak CR value is obtained for templates corresponding to the 4th to the 10th harmonics. The CR indices for the 5th to 9th templates are combined to derive an aggregate value RMS_t as shown in (11). Fig. 16(b) shows the RMS_t index. It can be seen that the RMS_t index has similar features to those of RMS_h . It can also be used for detection.

All three algorithms have been tested using field data, which eventually decides which algorithm is the best choice. The thresholds were selected based on field test results as well. The findings are reported in the companion paper.

VI. CONCLUSIONS

This paper has presented a new and powerful anti-islanding protection concept and associated scheme for DG applications. The scheme is similar to the telecomm-based transfer trip scheme. However, the signal is sent through power line, which makes the scheme applicable to any distribution systems regardless the availability of telecomm means. More importantly, since the signal passes through any switches, breakers and other openable components connected between the substation and DG sites; the scheme is able to ‘detect’ automatically the opening of any components. This has resulted in a significantly simplified ‘transfer trip’ scheme. In addition, the scheme is also economically attractive to DG owners and utilities, especially for systems with multiple DG installations.

This paper investigated the design considerations for the signal generator. A set of design formulas is established. Typical signal generator parameters are illustrated using actual system data. The proposed scheme can be implemented using other signalling techniques. Developing a signalling technique that can take advantage of the simple requirement of anti-islanding signalling to reduce the cost of signal generator is still a subject worth research.

The paper further investigated the characteristics of the anti-islanding signal. Key factors that can affect the signal strengthen, attenuation and frequency are identified. Based on the findings, three signal detection algorithms are proposed. The algorithms are tested using simulated waveforms.

ACKNOWLEDGMENT

The authors would like to thank the following companies and individuals: ATCO Electric (B. Howell, T. Palladino, S. Mathur, T. Parsons, and D. Flasha), Epcor Power Corporation (A. Mak, J. Byron), FortisAlberta Ltd. (R. Bahry), Enmax Corporation (B. Dreyer) and Dr. S. T. Mak. They would also like to thank the following current and former researchers of the University of Alberta power quality research group for their help: Y. Cui, X. Wang, S. Abdulsalam, M. Zha, and A. Terheide.

REFERENCES

- [1] “*IEEE Guide for Interfacing Dispersed Storage and Generation Facilities With Electric Utility Systems*,” ANSI/IEEE, 1988, IEEE/ANSI Std. 1001-1988.
- [2] *Recommendations for the Connection of Embedded Generating Plant to the Regional Electricity Companies Distribution Systems*, Std. G59/1, Electricity Assoc., 1991, Electricity Assoc. Std.

- [3] N. Jenkins, R. Allan, P. Crossley, D. Kirschen, and G. Strbac, *Embedded Generation*, 1st ed. London, U.K.: Inst. Elect. Eng., 2000.
- [4] W. Freitas, Z. Huang, and W. Xu, “A practical method for assessing the effectiveness of vector surge relays for distributed generation applications,” *IEEE Trans. Power Del.*, vol. 20, no. 1, pp. 57–63, Jan. 2005.
- [5] P. O. Kane and B. Fox, “Loss of mains detection for embedded generation by system impedance monitoring,” in *Development in Power System Protection*, *IEEE Conf. Publ.*, Mar. 1997, vol. 434, pp. 95–98.
- [6] M. E. Ropp, M. Begovic, and A. Rohatgi, “Prevention of islanding in grid-connected photovoltaic systems,” *Progr. Photovoltaics: Research and Applications*, vol. 7, no. 1, pp. 39–59, 1999.
- [7] C. J. Mozina, “Interconnection protection of IPP generators at commercial/industrial facilities,” *IEEE Trans. Ind. Appl.*, vol. 37, no. 3, pp. 681–689, May/June 2001.
- [8] W. Bower and M. Ropp, Evaluation Of Islanding Detection Methods For Photovoltaic Utility Int. Energy Agency, Rep. IEA PVPS T5-09, 2002 [Online]. Available: http://www.oja-services.nl/iea-pvps/products/download/rep5_09.pdf.
- [9] W. Xu, K. Mauch, and S. Martel, August 2004, An assessment of the islanding detection methods and distributed generation islanding issues for Canada. A report for CANMET Energy Technology Centre—Varennes, Nature Resources Canada, 65 pages. [Online]. Available: http://cetc-varennes.nrcan.gc.ca/fichier.php/39002/2004-074_e.pdf.
- [10] P. M. Foord, “Bi-Directional multi-frequency ripple control system,” U.S. Patent 4 868 539, Sep. 1989.
- [11] S. T. Mak and D. L. Reed, “TWACS, A new viable two-way automatic communication system for distribution networks. Part I: Outbound communication,” *IEEE Trans. Power App. Syst.*, vol. 101, no. 8, pp. 2941–2949, Aug. 1982.
- [12] S. T. Mak, “A new method of generating TWACS type outbound signals for communication on power distribution networks,” *IEEE Trans. Power App. Syst.*, vol. PAS-103, no. 8, pp. 2134–2140, Aug. 1984.
- [13] S. T. Mak and R. L. Maginnis, “Power frequency communication on long feeders and high levels of harmonic distortion,” *IEEE Trans. Power Del.*, vol. 10, no. 4, pp. 1731–1736, Oct. 1995.

Wilsun Xu (F’05) received the Ph.D. degree from the University of British Columbia, Vancouver, BC, Canada, in 1989.

From 1989 to 1996, he was an Electrical Engineer with BC Hydro, Vancouver and Surrey, respectively. Currently, he is with the Department of Electrical and Computer Engineering, University of Alberta, where he has been since 1996. His research interests are power quality and distributed generation.

Guibin Zhang received the B.Sc. and M.Sc. degrees in electrical engineering from Shandong University, Jinan, China, in 1995 and 1998, respectively, and the Ph.D. degree from Zhejiang University, Hangzhou, China, in 2001.

Currently he is with the AMC Technologies Corporation, Edmonton, AB, Canada. His main research interests are power quality, HVDC, and FACTS.

Chun Li (S’99–M’01) received the B.Eng. and Ph.D. degrees in electrical engineering from Tsinghua University, Beijing, China, in 1996 and 2000, respectively.

Currently, he is with the Asset Management Department of Hydro One Inc., Toronto, ON, Canada, working on power system transients, electromagnetic induction, insulation coordination, etc. Prior to joining Hydro One, he was a Postdoctoral Fellow in the Electrical and Computer Engineering Department, University of Alberta, Edmonton, AB, Canada.

Wencong Wang (S’05) received the B.E. and M.Sc. degrees in electrical engineering from Tsinghua University, Beijing, China, in 1999 and 2003, respectively, and is currently pursuing the Ph.D. degree in the Electrical and Computer Engineering Department, University of Alberta, Edmonton, AB, Canada.

Her research interests are distributed generation-related subjects and ground fault detection in non-effectively grounded distribution systems.

Guangzhu Wang (M'02) received the B.Sc. degree in electrical engineering from Xi'an University of Architecture and Technology, Xi'an, China, in 1984, and the M.Sc. degree in control engineering from Harbin Institute of Technology, Harbin, China, in 1987.

He has been with the faculty with the School of Electrical Engineering, Shandong University, Jinan, China, since 1987. In 2003, he was a Visiting Professor with the Electrical and Computer Engineering Research Facility, University of Alberta, Edmonton, AB, Canada. His research interests include analysis and control of power converters, active power filters, multilevel converters, power quality, power cable fault location, and fault detection in distribution systems.

Jacek Klüber (S'06) received the B.Sc. degree in electrical engineering from Queen's University, Kingston, ON, Canada, in 2004 and is currently pursuing the M.Sc degree in the Electrical and Computer Engineering Department at the University of Alberta, Edmonton, AB, Canada.

His research interests are related to distributed generation and power quality.

A Power Line Signaling Based Scheme for Anti-Islanding Protection of Distributed Generators—Part II: Field Test Results

Wencong Wang, *Student Member, IEEE*, Jacek Kliber, *Student Member, IEEE*, Guibin Zhang, Wilsun Xu, *Fellow, IEEE*, Blair Howell, and Tony Palladino

Abstract—Anti-islanding protection of distributed generators (DG) is a significant technical barrier to the emerging DG industry. In response to this challenge, a power line signaling based anti-islanding protection scheme has been proposed in a companion paper. The scheme broadcasts a signal from a substation to the DG sites using the distribution feeders as signal paths. A DG is considered as islanded from the upstream system if the signal is not detected at the DG site. This paper presents extensive field test results and experiences obtained for the proposed scheme. The results confirm that the proposed scheme is a very promising and economical method to satisfy anti-islanding protection requirements for synchronous DG interconnections.

Index Terms—Distributed generation (DG) interconnection, distributed generation, islanding, protection.

I. INTRODUCTION

DISTRIBUTED GENERATION (DG) has recently gained a lot of momentum in the power industry due to market deregulation and environmental concerns. An important requirement to interconnect a DG to power distribution systems is the capability of the generator to detect island conditions. Islanding occurs when a portion of the distribution system becomes electrically isolated from the remainder of the power system, yet continues to be energized by distributed generators. Failure to trip islanded generators can lead to a number of problems to the generators and the connected loads. Current industry practice is to disconnect all distributed generators immediately after the formation of islands [1], [2]. Typically, a distributed generator should be disconnected within 100 to 300 ms after loss of main supply.

Over the past several years, anti-islanding protection for DG has emerged as one of the most challenging technical

barriers for DG interconnection. Many research projects have been conducted to solve the problem worldwide [3], [4]. Until recently, there is still no reliable and economical solution to prevent distributed synchronous generators from sustaining unintended electrical islands.

Through more than three years of research effort, the authors have developed an innovative anti-islanding scheme. The scheme continuously broadcasts a signal from the utility substation to the downstream DGs. As a result, it transforms the detection of islanded DGs into the check of signal continuity between substation and DG sites. The scheme is developed mainly for synchronous generators but it is also applicable to other types of DGs. Key features of the scheme and its performance analysis have been presented in a companion paper [6].

The objective of this paper is to present extensive field test results on the proposed anti-islanding scheme. A prototype signal generator and detector were constructed in 2003 at the University of Alberta. They were installed in the distribution system of ATCO Electric Ltd., an Alberta utility company, for field tests and evaluation. The prototypes were tested for more than 6 months in 2004 from January to March and from September to October. A lot of valuable information was collected on the characteristics of signal propagation, performance of signal detection algorithms and even the interference of the proposed scheme with an AMR system.

This paper is organized as follows. Section II explains the field test arrangement including key information on the prototype device. Section III presents main findings of the field tests. Section IV analyzes the results and evaluates the proposed signal detection algorithms using the field data. Section V presents observations on the tests that were designed to determine the interference between the proposed scheme and the TWACS AMR scheme.

II. FIELD TEST ARRANGEMENT

The general arrangement of the field test is shown in Fig. 1. A prototype signal generator (SG) was connected to the 25 kV bus of a 216 fault MVA substation through a three-phase 300 kVA, 25 kV/480 V step down (signal) transformer. A prototype signal detector (SD) implemented on a laptop-based Labview platform was installed at a 347 V bus of a pipeline pumping station about 10 km away.

A picture of the signal generator installed at the substation is shown in Fig. 2. The signal generator is designed to fire the thyristor at 5, 10, 15, and 20° at the negative-going voltage zero-

Manuscript received April 3, 2006; revised June 7, 2006. This work was supported in part by the Alberta Energy Research Institute and in part by four utility companies in Alberta (ATCO, Epcor, Enmax, and FortisAlberta). Paper no. TPWRD-00175-2006.

W. Wang, J. Kliber, G. Zhang, and W. Xu are with the Department of Electrical and Computer Engineering, University of Alberta, Edmonton, AB T6G 2V4, Canada (e-mail: wwang@ece.ualberta.ca; jkliber@ualberta.ca; wxu@ee.ualberta.ca).

B. Howell is with ATCO Electric Ltd., Nisku, AB T9E 7S5, Canada (e-mail: blair.howell@atcoelectric.com).

T. Palladino is with ATCO Electric Ltd., Edmonton, AB T5J 2V6, Canada (e-mail: tony.palladino@atcoelectric.com).

Color versions of one or more of the figures in this paper are available online at <http://ieeexplore.ieee.org>.

Digital Object Identifier 10.1109/TPWRD.2007.899620

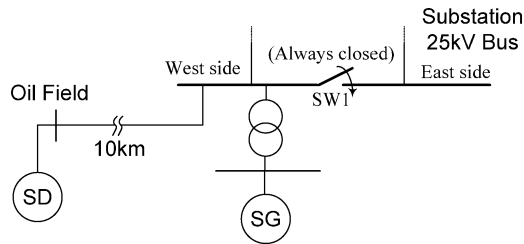


Fig. 1. Field test arrangement.



Fig. 2. Signal generator installed at the substation.

crossing point. The signals can be sent between phase to ground or phase to phase. Based on the system parameters, the signal strengths are estimated as 2.5% for phase to ground signaling and 2.1% for phase to phase signaling respectively at $\delta = 20^\circ$ and for phase to ground signal reception. For the test results reported in the subsequent sections, the SG sent signals using the phase to phase channel and $\delta = 20^\circ$. For this signaling arrangement, the thyristor peak current is estimated as 1382 A. It was a concern that such a high current could cause excessive temperature rise if the thyristors are fired too frequently. As a result, a signaling pattern of firing once every four cycles was used. The thyristor RMS current is about 168 A.

The signal detector is designed to operate with the 4-cycle signaling pattern. Four consecutive cycles is defined to be one signaling period. If a signal is absent for 3 continuous signaling periods, i.e. 12 cycles, an “islanding event” is detected. This means that the delay time for islanding detection is 12 cycles or 200 ms. If the signal is absent originally for three signaling periods but is detected for next three consecutive signaling periods, the event is considered as the starting of DG and a “starting event” is detected. With this design, an individual abnormal signal (definition see [6]) does not cause starting or islanding event. But if the signals are abnormal for three continuous periods or the signals are normal but their pattern does not follow the signal generation pattern, a warning event is recorded and 24 cycles of data are saved for offline analysis. The built-in signal detection algorithm was the RMS algorithm. This algorithm was the first one conceived for the project. It is therefore the only one implemented for the field test. The other two algorithms (spectrum and template [6]) were developed after the field test to overcome the problems encountered by the RMS algorithm.

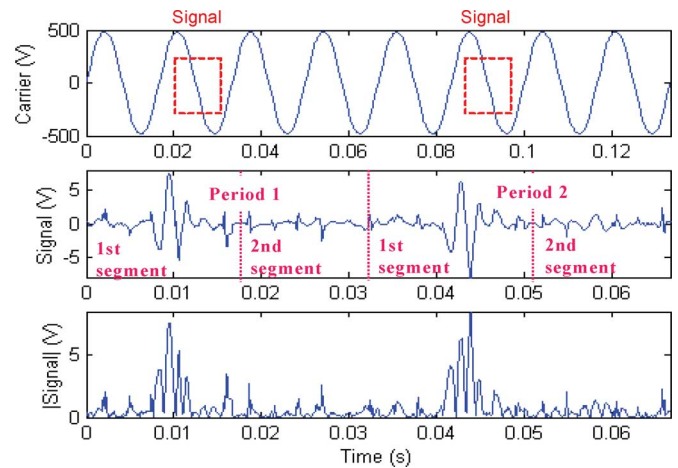


Fig. 3. Sample voltage waveform and anti-islanding signal waveform.

TABLE I
SUMMARY OF FIELD TEST RESULTS

Test Period	Duration	Threshold RMS (V)	“Nuisance islanding” events detected
I	67 hours	1.5	3
II	24 hours	1.5	0
III	31 hours	1.5	1
IV	24 hours	1.5	0

During the field test, the signal peak value was also tested as a detection index. Field experience show that the peak value was very sensitive to noise and the peak index was abandoned.

III. SUMMARY OF FIELD TEST RESULTS

The field tests were conducted in the spring and fall of 2004. The most useful results were obtained during the fall test. Sample voltage and signal waveforms recorded for this test are shown in Fig. 3. It can be seen that the signal is invisible from the voltage waveform, implying that the signal has little impact on power quality. The signal waveform v_{signal} was extracted by subtracting the 1st cycle by the 2nd cycle, the 3rd cycle by 4th cycle and so on of the carrier (voltage) waveform. Since the voltage waveform has eight cycles, the signal plot contains two signaling periods. Each period has two segments. One of them contains the signal and the other doesn't. For the plot shown in the figure, the signal is in the first segment. The figure also plots $|v_{signal}|$ which is used for signal strength determination and for signal detection.

Table I summarizes the main results using RMS based signal detection algorithm. The signal generator was turned on for four periods. As expected, all SG turn-off events, which represent genuine “islanding events,” have been correctly detected. The main concern here is if the signal detector could cause nuisance trips of a DG due to the inability to detect the existence of the SG signals. It can be seen from Table I that a total of four nuisance “islanding” events occurred. This implies that the signal detector failed to detect the presence of the signal for some of the signaling periods. The threshold used for detection is also listed in Table I. Note that the peak of the carrier voltage is 480 V. So the RMS threshold is about 0.3% of the rated voltage peak.

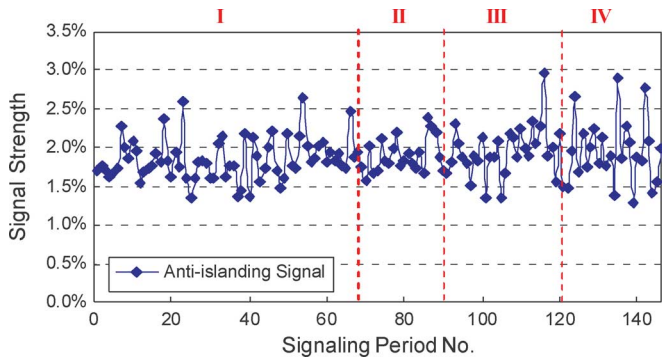


Fig. 4. Signal level during the field test period.

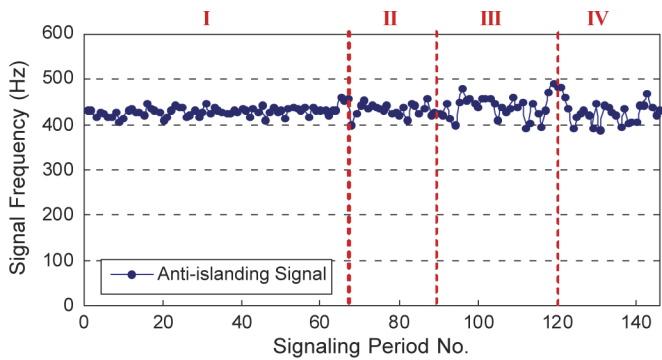


Fig. 5. Dominant signal frequency during the field test period.

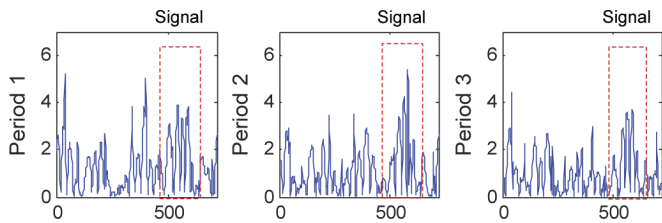


Fig. 6. Example of measured anti-islanding signal (Sep. 26, 00:01:22).

Figs. 4 and 5 show the signal strength (the k -index of [6]) and dominant signal frequency during the test period respectively. The data points are determined as follows: 1) a 16 cycles of waveform representing four signalling periods are selected randomly within every one-hour window; 2) signal strength for each signalling period is then determined, which yields four values; and 3) these four values are averaged to arrive at one data point. So each point of the figure represents one hour.

An example of waveforms that result in nuisance “islanding” events is shown in Fig. 6. This figure shows that the signals are not strong enough for the 1st, 2nd, and 3rd periods. Therefore, the cause for the above nuisance islanding events is identified as a weak signal along with high noise. The signal peak is only about 5 V or 1% in this case. The average signal strength in peak is about 1.9% (Fig. 4). The 1% signal level is too low to be detected by the RMS detection algorithm.

It is not clear, however, why the signal level dropped to 1% from a typical value of 1.9%. Fig. 4 does confirm that the signal strength varied during the test period. Such a phenomenon needs to be investigated further. One solution to the nuisance “islanding” detection problem is to increase the signal level to

about 3% to 4%. Improvement of the signal detection algorithm and/or increasing signaling periods will also help. This subject will be discussed in the next section.

The field test also showed that disturbances or noises may present themselves as signals even if the SG is actually offline. In this case, the SD will incorrectly record such events as the starting of the signal generator. This problem is mitigated by improving the verification of the uniformity of the signal pattern for several signal periods. As a result of this improvement, most nuisance starting events have been eliminated as well.

The field test task also evaluated various warning events recorded. The findings are omitted due to space limitation. Main conclusions drawn from this field test are summarized as follows.

- All SG shut off events which represent genuine “islanding” cases have been detected correctly.
- The SD failed to detect the presence of the anti-islanding signal for 4 occasions. This means that the nuisance trips of DG could occur. There is a need to address this issue.
- The average level of the signals is about 1.9%, which is consistent with the estimated level of 2.1%. However, the signal level fluctuates. The cause is not clear at present. More field measurement is needed.
- The signal frequency does not have significant variations during the test period. The frequency is around 430 Hz. This characteristic is important for the spectrum and template based signal detection algorithms.

IV. EVALUATION OF ALTERNATIVE SD ALGORITHMS

The spectrum and template based signal detection algorithms were proposed in response to the poor performance of the RMS based algorithm. The algorithms have been described in the companion paper [6]. In this section, they are evaluated using about 18 400 signalling periods recorded during the field tests. These periods were recorded because they have low signal levels that lead to warning events or false ‘islanding’ detection. To test the robustness of the template-based algorithm, the templates are aligned at the instant corresponding to a firing angle of 30°, which is slightly different from the actual firing angle of 20°.

1) *Typical Performance*: A set of normal signalling periods is used as an example to show how the algorithms’ performance is assessed. Recall that each signalling period consists of two segments of signal waveforms (Fig. 3). One of them contains the signal. RMS_h and RMS_t are calculated for both segments. The results corresponding to the signal-containing segment is labelled as ‘with signal’ and those corresponding to the no-signal segment are labelled as ‘without signal’. The results are shown in Fig. 7. For reliable signal detection, the two sets of (RMS) values should be far apart. The vertical separation of the two curves shows the ability of an algorithm to distinguish signals from noises. For the results shown in Fig. 7, there is a clear separation between the segments with signal and those without signal. A detection threshold of, say, 1.2 V (for the spectrum method) and 15 p.u. (for the template method) can be used to detect the signal easily.

2) *Performance With Respect to Four Nuisance Islanding Events*: Waveforms recorded for the 4 false “islanding” events that could cause nuisance DG trips were analyzed in detail.

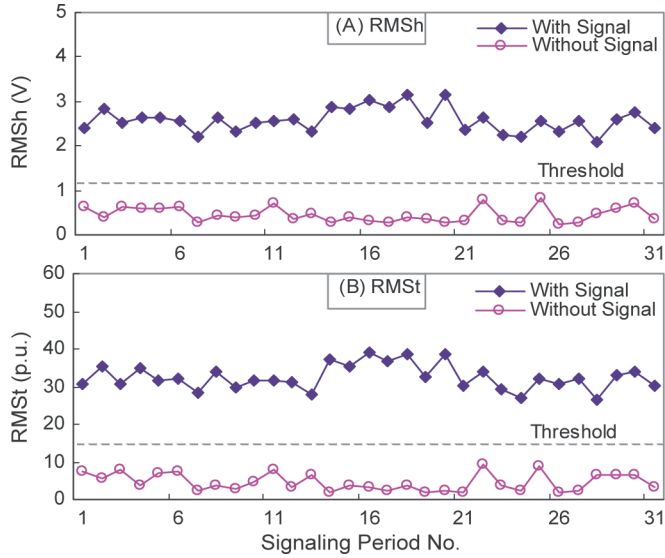


Fig. 7. RMS_h and RMS_t of signaling/non-signaling cycles from 31 records.

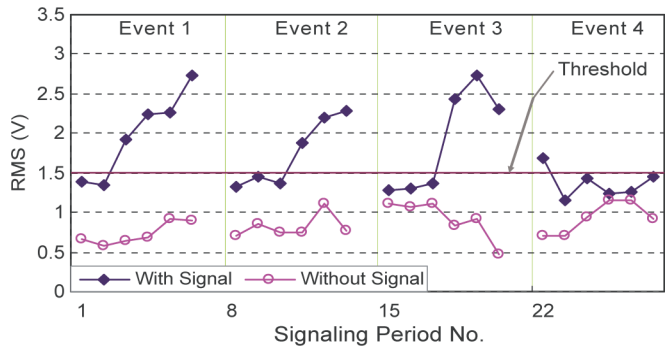


Fig. 8. Performance of the RMS algorithm.

Figs. 8–10 show the signal characteristics when different detection algorithms are applied to the data. According to Fig. 8, it is very hard to separate the signal-containing data from the non-signal data. This is especially true for event 4. The findings explain why the RMS algorithm will lead to false islanding detection for the signalling periods. In comparison, indices RMS_h and RMS_t show improved separation between the signals and noises. There will be no nuisance “islanding” detection according to the new algorithms. When these algorithms are used, the false islanding detection events are eliminated.

3) *Statistical Signal Strength Analysis*: To understand the statistical performance of three detection algorithms, all 18 400 signalling periods are played back to the algorithms. The results are shown in Figs. 11–13. To avoid crowding caused by massive amount of data points, the plots just show the points sampled from the original results at a rate of 1 sample per 12 data points. It can be seen that the signal strength is generally constant for the test duration. However, there is a large fluctuation of signal strength for period IV. Some of the high signal cases were analysed and the cause was found to be AMR interference (see next

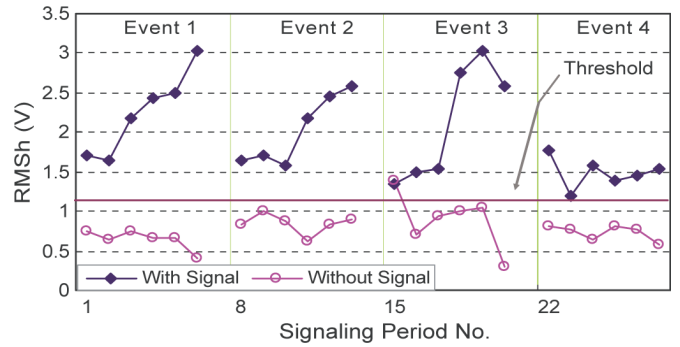


Fig. 9. Performance of the spectrum based algorithm.

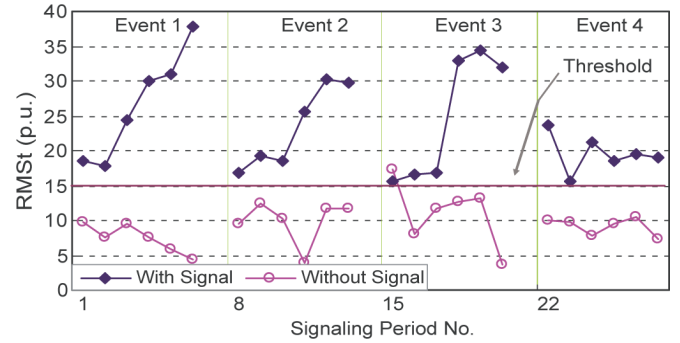


Fig. 10. Performance of the template based algorithm.

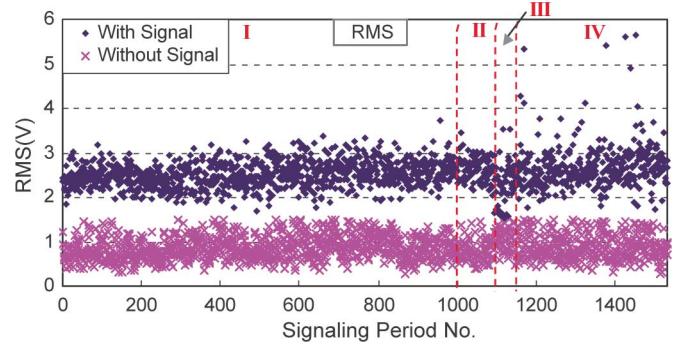


Fig. 11. Statistical performance of the RMS based algorithm.

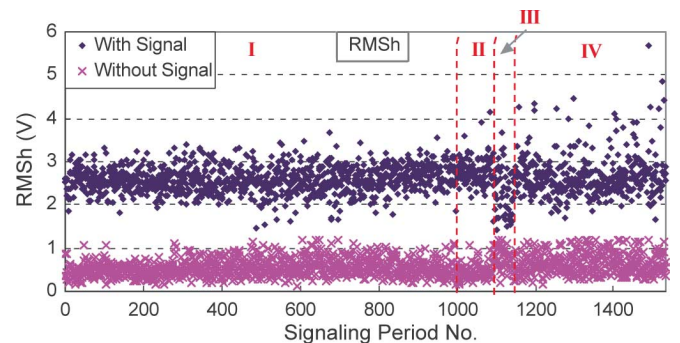


Fig. 12. Statistical performance of the spectrum based algorithm.

section). For the period III, the signal level is lower than average. The causes have not been found.

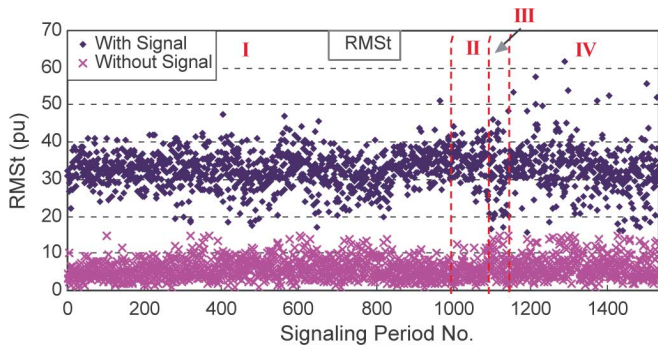


Fig. 13. Statistical performance of the template based algorithm.

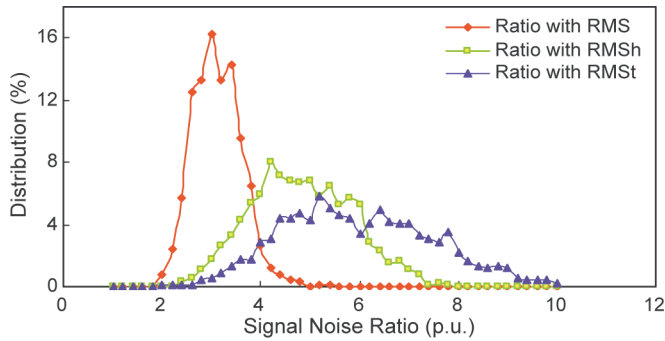


Fig. 14. Distribution of the signal noise ratio of RMS , RMS_h , and RMS_t .

To quantify the signal detection capability of different algorithms, an index of signal to noise ratio is determined. The ratio is defined as

$$\text{Signal Noise Ratio} = \frac{RMS_{withSignal}}{RMS_{nonSignal}} \quad (1)$$

Fig. 14 shows the statistical distribution of the ratio index. According to the figure, the average signal to noise ratios of RMS , RMS_h and RMS_t are about 3, 4.5 and 6 respectively. A higher ratio means that the corresponding algorithm can detect the signal more reliably. The results confirm the observation that the RMS based algorithm has the poorest performance. Note that although the ratio of RMS_t has the highest average, it distributes in a wider range than the other two ratios. In the worst case, the ratio of RMS_t drops to 2.8 and is close to the worst case of RMS_h .

Based on the above results, we can conclude that the spectrum and template based algorithms have better performance than the RMS algorithm. There is no significant performance difference between the spectrum and template based algorithms. Either of them can be selected for implementation. However, the algorithms have different computational burden, which becomes a deciding factor.

V. INTERFERENCE OF ANTI-ISLANDING AND AMR SCHEMES

The proposed anti-islanding scheme adopts the waveform distortion technique for signaling [6]. The same technique has also been applied for automatic meter reading (AMR) [5] and load control applications. The potential interference between

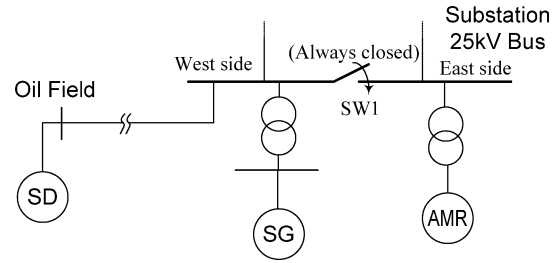


Fig. 15. Parallel operation of anti-islanding and AMR schemes.

the anti-islanding and the AMR schemes becomes a natural concern. Understanding the nature and degree of inference is critical to the acceptance of the proposed anti-islanding scheme by industry. Fortunately, the ATCO Electric is the first utility company that deployed the waveform distortion based AMR scheme. As a result, the project had the opportunity to evaluate the interference concern. The test set up for this study is shown in Fig. 15.

The AMR system was running concurrently with the SG during test periods II and IV. Note that the AMR system also sends signals occasionally even if no meter reading takes place. The purpose is to calibrate time for the revenue meters. Test periods I and III were run under such condition. For all test periods, the channels used by the AMR were essentially random. Main findings from these tests are as follows.

- When the SG is ON, the AMR signal caused SD to detect warning events. A number of warning events were captured during the period IV. This is due to the following reason: if the AMR signal appears at the same waveform location as the anti-islanding signal (say negative-going zero-crossing point) and it is in a cycle ahead of the anti-islanding signal cycle, the subtraction of the two adjacent cycles will show no signal or very weak signal. As a result, the anti-islanding signal may not be detected. For the same reason, the AMR signal may also strengthen the anti-islanding signal. The high signal level recorded in period IV is due to this cause.
- When the SG is OFF, AMR signals resulted in warning and even starting events. This is due to the fact that the signal detector treats the AMR signal as the anti-islanding signal mistakenly.
- Theoretically, the AMR signals could cause nuisance DG trips by “erasing” the anti-islanding signal. For such events to happen, the AMR signal must have a pattern complement to that of the anti-islanding signal so that the subtraction of two waveform cycles result in null signal. This is a low probability event and it was not encountered in the field.

In summary, the impact of the AMR signal on the proposed anti-islanding scheme is not significant. This is because the AMR has not caused nuisance “islanding” detection when the SG is ON. It only caused warning events. Furthermore, if a SG is put into operation to send anti-islanding signals, a lack of a SG signal means islanding has happened. The AMR signal won’t be able to reach the DG site either. As a result, AMR signal cannot sustain an island. So we can conclude that the AMR is very unlikely to cause interference to the anti-islanding scheme.

It is likely that the anti-islanding signal will affect the operation of the AMR system. The experience of the ATCO Metering Department during the test did not suggest that such interference has happened. The AMR system worked smoothly during the entire field test. One of the explanations may be that the AMR signal at 4% is much stronger than the anti-islanding signal that is at 1.9%. However, a lot more field tests are needed to confirm if the anti-islanding signal is indeed troublesome to AMR. Should interference exist, one of the solutions is to let the AMR signal transmitter broadcast both meter reading and anti-islanding signals but using different signaling channels.

VI. CONCLUSIONS

This paper has presented field results and their analysis for a novel DG islanding detection scheme. The field test arrangement and device settings are explained. The main findings from the field test study are as follows.

- The proposed scheme performed successfully during the field test. The four false islanding events encountered during the test can be eliminated using improved signal detection algorithms.
- The improved algorithms, either spectrum-based or template based, are more reliable for signal detection. They are recommended for uses in the signal detector of the proposed scheme. The degree of implementation (programming) difficulties will decide which one of them will be selected eventually.
- Investigation on the interference between the AMR and anti-islanding schemes shows that the AMR system is unlikely to cause problems to the anti-islanding scheme. Although field experience suggests that the anti-islanding scheme did not interfere with the AMR system, more field test is needed to clarify this issue.
- The field test experience suggests that a signal level of 4% is probably the best compromise between reliable signal detection and the cost of signal generator. Power quality is not a concern at this signal level.

ACKNOWLEDGMENT

The authors would like to thank the organizations and individuals who have supported this project technically and/or financially during the past four years: ATCO Electric (S. Mathur, T. Parsons, and D. Flasha), Epcor Power Corporation (A. Mak, J. Byron), FortisAlberta Ltd. (R. Bahry), Enmax Corporation (B. Dreyer) and Dr. S. T. Mak. The following current and former researchers of the University of Alberta power quality research group are also fully acknowledged: C. Li, G. Zhang, Y. Cui, X. Wang, S. Abdulsalam, M. Zha, and A. Terheide.

REFERENCES

- [1] *IEEE Guide for Interfacing Dispersed Storage and Generation Facilities With Electric Utility Systems*, IEEE/ANSI Std. 1001-1988.
- [2] Electricity Assoc., G59/1 recommendations for the connection of embedded generating plant to the regional electricity companies distribution systems Electricity Assoc. Std., 1991.

- [3] W. Bower and M. Ropp, Evaluation of islanding detection methods for photovoltaic utility Int. Energy Agency, Rep. IEA PVPS T5-09, 2002. [Online]. Available: http://www.oja-services.nl/iea-pvps/products/download/rep5_09.pdf.
- [4] W. Xu, K. Mauch, and S. Martel, August 2004, An assessment of the islanding detection methods and distributed generation islanding issues for Canada, A report for CANMET Energy Technology Centre—Varennes, Nature Resources Canada, 65 pages. [Online]. Available: http://www.cetc-varennes.nrcan.gc.ca/fichier.php/39002/2004-074_e.pdf.
- [5] S. T. Mak, "A new method of generating TWACS type outbound signals for communication on power distribution networks," *IEEE Trans. Power App. Syst.*, vol. PAS-103, no. 8, pp. 2134–2140, Aug. 1984.
- [6] W. Xu, G. Zhang, C. Li, W. Wang, G. Wang, and J. Kliber, A power line signaling based technique for anti-islanding protection of distributed generators—Part I: scheme and analysis a companion paper submitted for review.

Wencong Wang (S'05) received the B.E. and M.Sc. degrees in electrical engineering from Tsinghua University, Beijing, China, in 1999 and 2003, respectively, and is currently pursuing the Ph.D. degree in the Electrical and Computer Engineering Department, University of Alberta, Edmonton, AB, Canada.

Her research interests are distributed generation-related subjects and ground fault detection in non-effectively grounded distribution systems.

Jacek Kliber (S'06) received the B.Sc. degree in electrical engineering from Queen's University, Kingston, ON, Canada, in 2004 and is currently pursuing the M.Sc. degree in the Electrical and Computer Engineering Department at the University of Alberta, Edmonton, AB, Canada.

His research interests are related to distributed generation and power quality.

Guibin Zhang received the B.Sc. and M.Sc. degrees in electrical engineering from Shandong University, Jinan, China, in 1995 and 1998, respectively, and the Ph.D. degree from Zhejiang University, Hangzhou, China, in 2001.

Currently he is with the AMC Technologies Corporation, Edmonton, AB, Canada. His main research interests are power quality, HVDC, and FACTS.

Wilsun Xu (F'05) received the Ph.D. degree from the University of British Columbia, Vancouver, in 1989.

From 1989 to 1996, he was an Electrical Engineer with BC Hydro at Vancouver and Surrey, respectively. Currently, he is with the Department of Electrical and Computer Engineering, University of Alberta, where he has been since 1996. His research interests are power quality and distributed generation.

Blair Howell received the B.Sc. degree in electrical engineering from the University of Saskatchewan, Saskatoon, SK, Canada, in 1982.

Currently, he is Superintendent of Distribution Standards and Operations with ATCO Electric Ltd. and has more than 20 years of experience with electric utility operations, distribution planning, and the design of power system facilities. He has extensive experience in the successful interconnection of generators to ATCO Electric's distribution system, and was involved throughout the entire process of developing Alberta's Distributed Generation Interconnection Guide.

Tony Palladino received the B.Sc. degree in electrical engineering from the University of Alberta, Edmonton, AB, Canada, in 1977.

He has 29 years of experience in the electrical utility business, primarily in distribution engineering and marketing. Since joining ATCO Electric (formerly Alberta Power Ltd.) in 1977, he has been responsible for planning, design, and project management of the company's distribution systems, and has been involved in the regulatory changes as the industry transitions into wholesale and retail deregulation. During the project field test period, he was a Senior Manager of Customer Services of ATCO, where he is currently Manager of Human Resources.

For more information on these or other
products & services email us at:

sales@enertiaengineering.com



Unit #105, 117 Pembina Road
Sherwood Park, AB, Canada
T8H 0J4

Phone: 780-467-0303
Toll Free: 866-796-0303
Fax: 780-401-3519

7 Cedar Street, Suite 203
Sudbury, ON, Canada
P3B 4H5

Phone: 705-693-4829
Toll Free: 1-877-693-482

627A Aljunied Road
#04-01 BizTech Centre
Singapore 389842

Phone: (65) 64814106